

# The sensors for the intelligent micro washing system

## Elimination of the glass reference electrode with amperometry

Work report 11, 27-Mar-99

Geert Langereis

<b>1. Preface .....</b>	<b>2</b>
<b>2. Introduction .....</b>	<b>3</b>
2.1 The Pourbaix diagram.....	3
2.2 Controlled potential measurement techniques.....	5
<b>3. Experimental .....</b>	<b>9</b>
3.1 Three electrode set-up.....	9
3.2 Two electrode set-up.....	11
3.3 Conclusions.....	12
<b>4. Some additional comments on the conductivity-temperature technique .....</b>	<b>13</b>
4.1 Measurement of the error distribution curve.....	13
4.2 Absolute errors in the fitted ion concentrations .....	15
<b>5. Future work.....</b>	<b>18</b>
5.1 What has to be done.....	18
5.2 Outline of the thesis .....	20
<b>A. References.....</b>	<b>22</b>
<b>B. Distribution list.....</b>	<b>22</b>

## 1. Preface

Work report 9 described the design, development and measurements of a multi purpose integrated sensor structure. With this structure some parameters could be measured and locally changed by selecting certain operational modes. Of all mentioned operational modes, only one required an external reference electrode. The Ag/AgCl glass reference electrode used for the chrono-amperometric detection of a bleaching component is obviously a weak aspect in the sensor array.

This work report shows a method for eliminating this less elegant element in the sensor array. The probe part of the sensor array system is now being reduced to a PCB dip-stick with a silicon chip on top and an inert metal counter/pseudo reference electrode on the backside.

## 2. Introduction

*This section summarises some theory and the progresses that were made for sensing bleach activity using an amperometric working electrode. Hydrogen peroxide was used as a representative bleaching agent for evaluating the measurement techniques. The final result will be a two electrode set-up with which the bleach activity can be monitored after interpreting the measured current sweep.*

### 2.1 The Pourbaix diagram

Although a sensing method is derived for measuring bleach activity in general, hydrogen peroxide is used as model for bleaching agents. An elegant representation for the reaction and equilibrium formulas of hydrogen peroxide is a Pourbaix diagram [1]. This diagram contains information on both the acid-base behaviour and electrochemical reactions, together plotted in a potential versus pH graph. All numerical values for the electrode potentials and acid or base constants were taken from [2].

#### *Acid base behaviour*

Decomposition of hydrogen peroxide to the intermediate hydrogen peroxide anion satisfies:



with the acid constant defined as:

$$k_a = \frac{[\text{HO}_2^-] \cdot [\text{H}^+]}{[\text{H}_2\text{O}_2]} = 2.4 \cdot 10^{-12} \quad (2.2)$$

from which it can be calculated that at pH = 10 the hydrogen peroxide is dissociated for only 2.3%. The logarithm of this equation yields the first equation for the construction of the Pourbaix diagram:

$$\log \frac{[\text{HO}_2^-]}{[\text{H}_2\text{O}_2]} = -11.63 + \text{pH}. \quad (2.3)$$

It appears that for pH = 11.63 the ratio  $[\text{HO}_2^-]/[\text{H}_2\text{O}_2] = 1$ .

#### *Electrochemical reactions*

For both  $\text{HO}_2^-$  and  $\text{H}_2\text{O}_2$  an electrochemical interaction with water and  $\text{H}^+$  can be observed:



with  $E^0$  the standard electrode potential. For electrolyte concentrations not equal to 1 molar and gas pressures not equal to 1 atmosphere, the standard electrode potentials must be transformed to the formal potentials  $E^0'$ . This results in the following potential/concentration dependencies:

$$E^0' = 1.776 + \frac{RT}{2F \log(e)} \log[H_2O_2] - \frac{RT}{F \log(e)} \text{pH} \quad (2.4b)$$

$$E^0' = 2.119 + \frac{RT}{2F \log(e)} \log[HO_2^-] - \frac{3RT}{2F \log(e)} \text{pH} . \quad (2.5b)$$

The electrochemical reactions of  $HO_2^-$  and  $H_2O_2$  with dissolved oxygen are:



with the corresponding potential/concentration equations:

$$E^0' = 0.695 + \frac{RT}{2F \log(e)} \log \frac{pO_2}{[H_2O_2]} - \frac{RT}{F \log(e)} \text{pH} \quad (2.6b)$$

$$E^0' = 0.338 + \frac{RT}{2F \log(e)} \log \frac{pO_2}{[HO_2^-]} - \frac{RT}{2F \log(e)} \text{pH} . \quad (2.7b)$$

### The Pourbaix diagram

When the equations (2.3), (2.4b), (2.5b), (2.6b) and (2.7b) are plotted into a single potential versus pH plot, assuming some values for the concentrations of  $O_2$ ,  $H_2O_2$  and  $HO_2^-$ , this plot is referred to as a Pourbaix diagram [1].

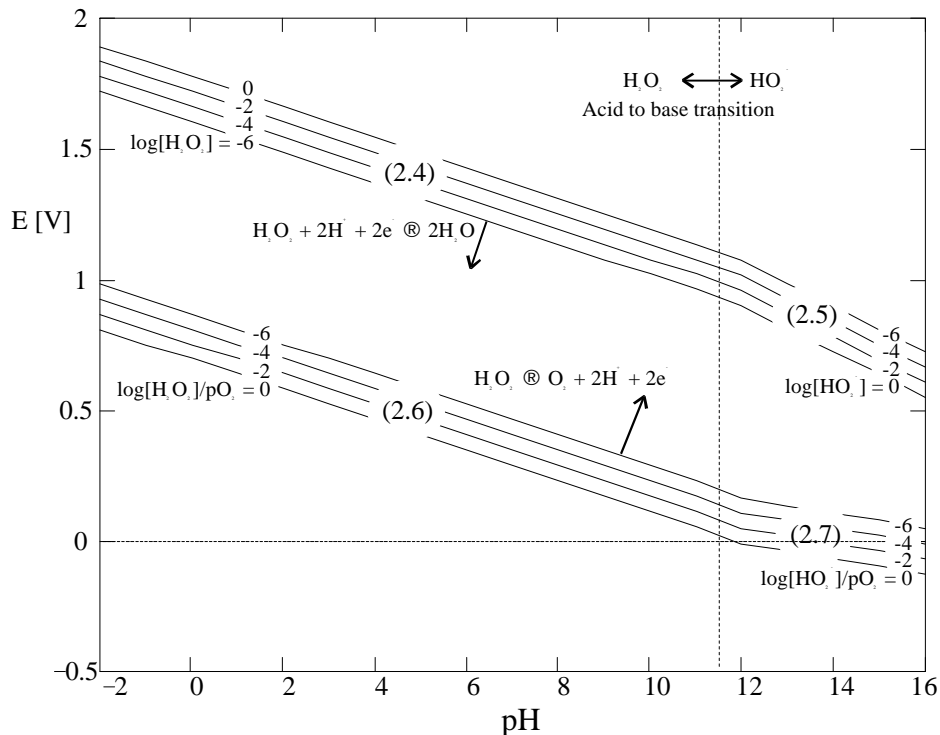
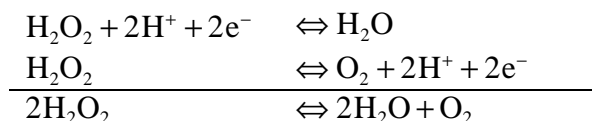


Figure 2.1: The Pourbaix diagram for the system  $H_2O_2$ -water at 25°C

From this graph it can be concluded that below the lines of the equation (2.4), hydrogen peroxide can act as an oxidising agent with the formation of water. In general, this is the bleaching effect of hydrogen peroxide where coloured stains are oxidised into soluble non-coloured elements.

Above the lines of the equation (2.6), hydrogen peroxide is a reducing agent with the formation of dissolved oxygen. These two domains have a common area, in which hydrogen peroxide is said to be double unstable and can decompose into water and oxygen.



So at a metallic surface with an electrode potential in the range of double instability, the decomposition of hydrogen peroxide is being catalysed. Because this decomposition process is much slower than electrochemical reactions involved with amperometric experiments, this phenomenon is not likely to be of interest during a measurement. The spontaneous decomposition of hydrogen peroxide without a catalytic electrode is even lower.

## 2.2 Controlled potential measurement techniques

The theory represented by the Pourbaix diagram can be used to measure hydrogen peroxide concentrations. Generally, this is done by dynamic measurements with a controlled potential, which means that the working electrode potential is swept from one area in the diagram to another while monitoring the current under non-stirring conditions.

A three electrode set-up is used for applying the desired potential across the working electrode/electrolyte interface as shown in Figure 2.2. No current flows through the reference electrode and in general, the working electrode is grounded.

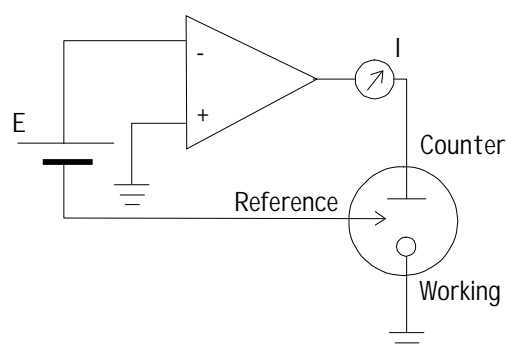


Figure 2.2: Three electrode set-up with potentiostat

The differences in the controlled potential techniques are in the applied potential signal and the way the measured current is represented.

### Chrono-amperometry

When crossing a state line in the Pourbaix diagram by making a potential step using a working electrode while monitoring the current is referred to as chrono-amperometry [3]. For example, when in Figure 2.1 an electrode is stepped from 0 to 1 Volt at pH = 8, only the lines (2.6) are crossed, so the observed current response is the result of equation (2.6a) finding its new equilibrium. The chrono-amperometric current response has a  $1/\sqrt{t}$  shape and is linearly dependent on the hydrogen peroxide concentration.

In work report 9 this technique was used with a platinum ( $0.50 \text{ mm}^2$ ) working electrode in a three electrode set-up with an Ag/AgCl reference electrode and a platinum counter electrode. The measurement set-up consisted of an EG&G potentiostat/galvanostat model 173 under computer control.

Hydrogen peroxide concentrations were used of 10, 20, 30, 40 and 50 mM, directly measured after dilution from a 80 wt% bulk solution. To prevent an ohmic drop across the sample, a background electrolyte of 10 mM  $\text{KNO}_3$  was used. The oxygen pressure was minimised by bubbling with nitrogen gas before the measurement.

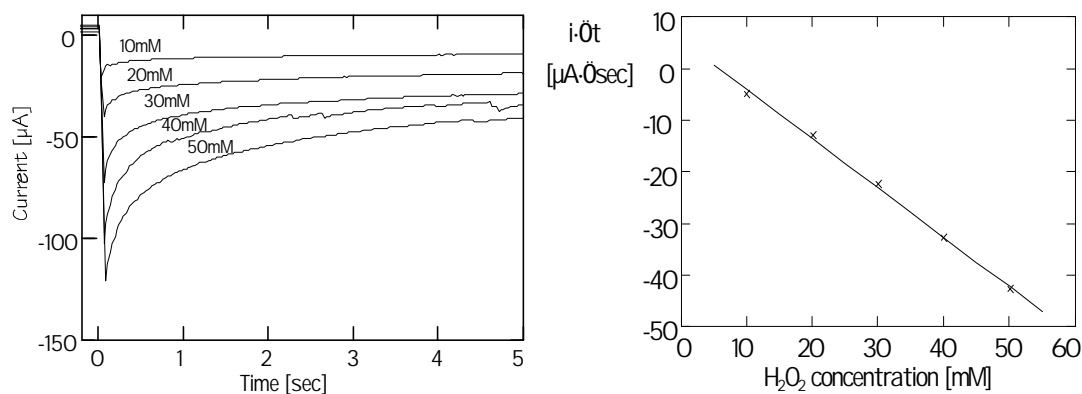


Figure 2.3: Chrono amperometric measurements (left) and the measured linear dependency of  $i\sqrt{t}$  on the  $\text{H}_2\text{O}_2$  concentration (right)

Figure 2.3 (left) shows the recorded current responses with the characteristic  $1/\sqrt{t}$  shape. A potential step of 1 Volt versus Ag/AgCl appeared to be sufficient for stepping from the area under the lines (2.6) in the Pourbaix diagram to the area above these lines, without crossing the lines (2.4). Since the current is dependent on  $1/\sqrt{t}$ , the product  $i\sqrt{t}$  is constant and only concentration dependent (right figure). This line does not go through the origin as expected (zero current for zero hydrogen peroxide concentration), but a small offset is observed. This is probably the result of the loading of the capacitive double layer.

### Sampled current voltammetry

In order to get the expected  $1/\sqrt{t}$  shape with the chrono-amperometric experiment, the applied end potential must be in a special range. When the end potential is too small ( $< E^0$ ) the measured current is dependent on this potential. About 0.7 volts above  $E^0$ , the current response becomes independent on the applied potential and the current is proportional to  $1/\sqrt{t}$ . However, when increasing the end potential too much, the

current is no longer determined by the oxidation of hydrogen peroxide but by the evolution of oxygen.

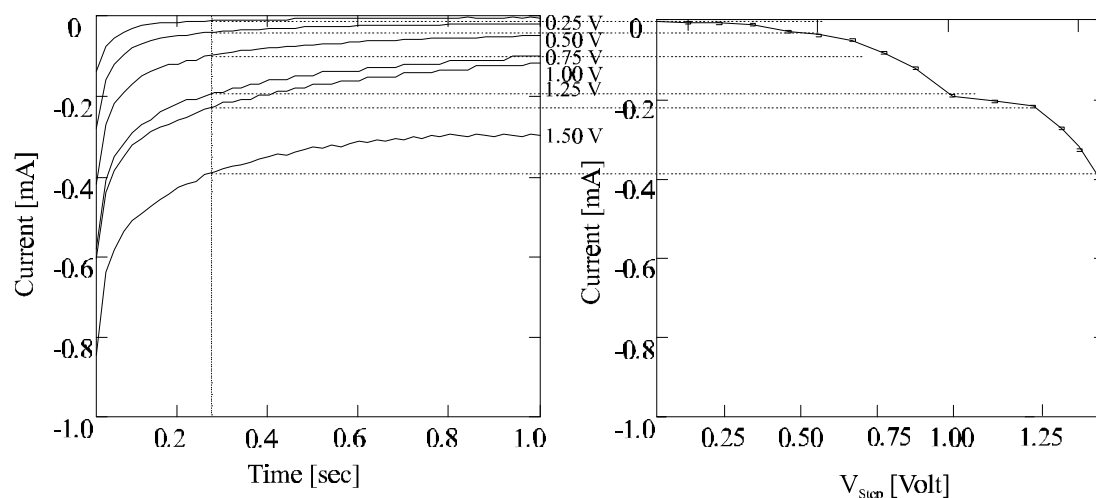


Figure 2.4: Chrono amperometric curves (left) in 100 mM  $\text{H}_2\text{O}_2$  at various potential steps and the sampled currents (right) after  $t = 0.3$  sec

Figure 2.4 (left) shows a number of chrono amperometric experiments at various potential step sizes. The electrolyte consisted of 100 mM  $\text{H}_2\text{O}_2$  with 50 mM  $\text{KNO}_3$  as a background electrolyte. A summary of the sampled currents after 0.3 seconds is given in the figure at the right. The mentioned three areas are clearly present: first the current is dependent on the step size, then there is a step size independent plateau suitable for chrono amperometry and then the potential is large enough for the electrolysis of water.

From this curve, which is commonly referred to as sampled current voltammogram, it becomes clear that the actual value of the applied potential is not of interest for a concentration measurement. When the plateau in Figure 2.4 (right) is detected, the chrono amperometric experiment is meaningful and the concentration can be calculated without knowing the absolute potential. So, if the stable  $\text{Ag}/\text{AgCl}$  reference electrode is being replaced by a simple platinum electrode, the voltammogram will shift an unpredictable potential along the potential axis but will still give the same information. Notice that this potential shift must remain constant for each chrono amperometric experiment. Probably, this condition is met in the three electrode set-up where no current flows through this platinum reference electrode, so no time or current dependent electrode potential is expected. The platinum electrode can probably act as a pseudo reference in a three electrode set-up.

#### *Potential sweep voltammetry*

A method that has some resemblance with sampled current voltammetry, is potential sweep voltammetry [3]. While with the sampled current technique a set of chrono amperometric experiments has to be done for constructing the voltammogram, sweeping the electrode potential linearly will give a potential-current curve directly. Although the mechanisms determining the shapes of sampled current and potential sweep methods are completely different, the possibility of substituting the decent reference electrode is mutual.

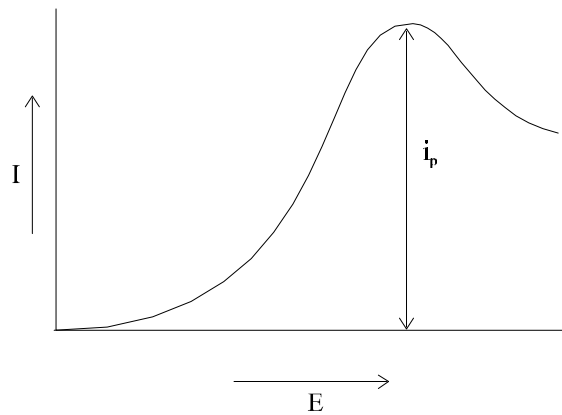


Figure 2.5: Typical shape of a linear cathodic sweep voltammogram for a reversible system

Because of the different kinetics the potential sweep technique shows no plateau's, but peaks. Figure 2.5 shows the typical shape of a cathodic linear sweep voltammogram. The peak current  $I_{\text{peak}}$  is determined by:

$$i_{\text{peak}} = kn^{3/2}AD_{\text{Ox}}^{1/2}v^{1/2}C_{\text{Ox}}^* \quad (2.8)$$

with:

- k the Randles-Sevcik constant being equal to  $2.69 \cdot 10^5 \text{ A} \cdot \text{s} \cdot \text{mol}^{-1} \cdot \text{v}^{-1/2}$ ;
- n the number of electrons involved in the reduction;
- A the electrode surface area;
- $D_{\text{Ox}}$  the diffusion constant of the particle to be reduced;
- v the potential sweep speed;
- $C_{\text{Ox}}^*$  the bulk concentration of the particles to be reduced.

The appearance of a peak in the current, while this was not the case with the sampled current voltammogram, is due to the depletion of the target particles near to the electrode surface. Because the diffusion layer thickness of the particles to be reduced increases with the applied potential, the mass flux rate decreases.

The use of this sweep technique appeared to be a more practical method for determining a reference point (plateau or peak) than the sampled current method. By measuring the current at the peak, the concentration indication becomes independent of the used reference electrode.

### 3. Experimental

The conclusion of the previous chapter was that it should be possible to measure the hydrogen peroxide concentration amperometrically without knowing the exact electrode potential. In this chapter some measurements are reported which verify this idea. The measurements were done in both a three and a two electrode set-up.

#### 3.1 Three electrode set-up

In a set-up with three electrodes like represented in Figure 2.2 some potential sweep methods were performed. The working electrode was a platinum film ( $0.50 \text{ mm}^2$ ) on a silicon substrate from which it was galvanically insulated by a  $1 \text{ }\mu\text{m}$  thick thermally grown silicon dioxide layer. A platinum plate of  $0.5 \text{ cm}^2$  was used as a counter electrode. For the reference electrode both a commercial Radiometer Ag/AgCl electrode and a second platinum  $0.5 \text{ cm}^2$  electrode were chosen. The measurements were performed by an EG&G potentiostat/galvanostat model 173 under computer control. Before each measurement, the solution was saturated with nitrogen gas in order to minimise the oxygen concentration. During the recording of a sweep, the solution was not stirred

The solid loop of Figure 3.1 shows the dominant reversible reaction in a measured CV. The reference electrode was Ag/AgCl and  $100 \text{ mM KNO}_3$  was applied for creating a high background electrolyte concentration. The scan rate was  $300 \text{ mV/sec}$ .

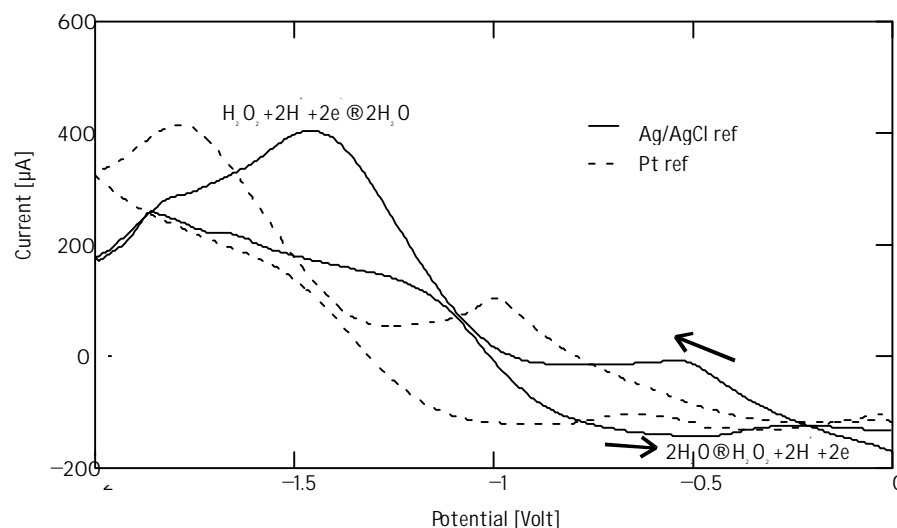


Figure 3.1: Cyclic voltammogram in  $0.1 \text{ M H}_2\text{O}_2$  with  $0.1 \text{ M KNO}_3$  as a background electrolyte

Remarkable is that the CV implies a cathodic current (reductive reaction), while the involved reversible reaction is probably (2.4a). This reaction should occur at a positive potential due to the given  $E^0$ . However, at dynamic measurements, like CV's, this potential shift is commonly observed because the given equations represent thermodynamic phenomena and do not include reaction kinetics. When using the CV

as a fingerprinting technique for locating a reaction peak, the absolute potential is not of interest and therefore no attempt is made here for completely understanding the shape of the curves.

Now the primary reaction was located in the CV using this fingerprinting method, the experiment was repeated with the reference electrode replaced by a simple platinum plate (dashed line in Figure 3.1). As predicted in theory, the shape of the CV is not changed, only the potential of the reference is shifted. So, although the platinum reference has an unknown electrode potential, this potential is at least constant during the potential sweep which took two seconds.

Next, this experiment was repeated for other concentrations of hydrogen peroxide. Only the parts of the sweeps from 0 to -2 volt are plotted in Figure 3.2, the scan rate was 500 mV/sec now. The peaks  $I_{\text{peak}}$  can easily be read from these curves and plotted into an  $I_{\text{peak}}$  versus  $\text{H}_2\text{O}_2$  concentration graph (Figure 3.3).

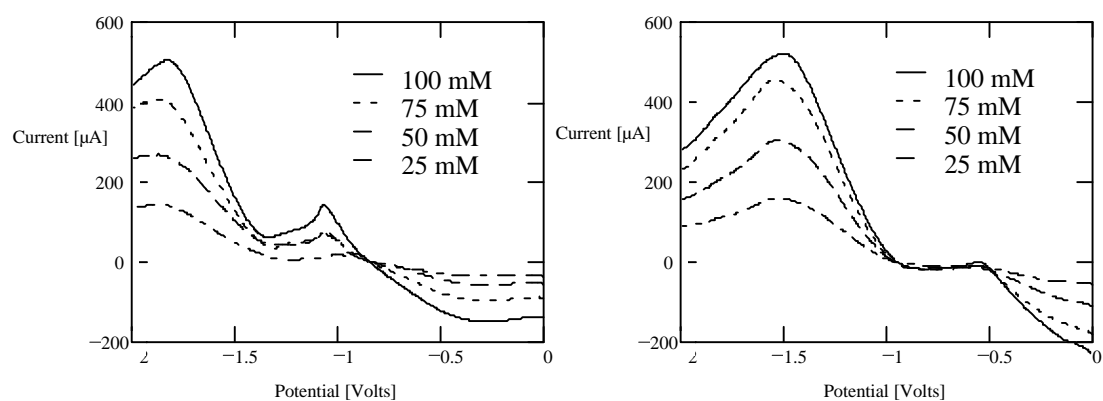


Figure 3.2: Potential sweep voltammograms in various concentrations  $\text{H}_2\text{O}_2$  with Ag/AgCl reference (left) and Pt reference (right)

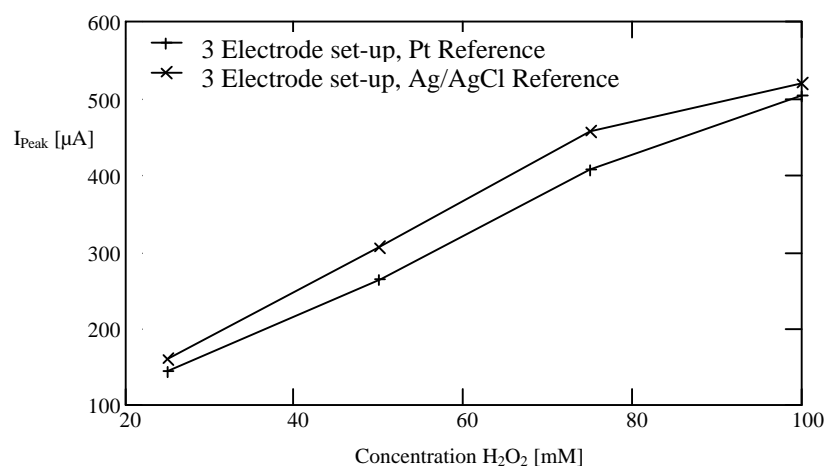


Figure 3.3: The measured values for  $I_{\text{peak}}$  as a function of  $\text{H}_2\text{O}_2$  concentration

The conclusion is that the height of the current peak is a good indication for the hydrogen peroxide concentration in these three electrode systems. It does not really matter what the reference electrode is.

### 3.2 Two electrode set-up

The advantage of a three electrode set-up is that the potential across the working electrode\electrolyte interface can be measured or applied directly. In a two electrode set-up, the measured or applied potential will be distributed over two electrode\electrolyte interfaces.

However, in the case of the current peak detection method, the knowledge of the separate interface potentials is not needed. In addition, the size of the counter electrode can be chosen much larger than the size of the working electrode which results in a much lower current density at this counter electrode. Therefore, it is not likely that the reactions at the counter electrode will be present significantly in the voltammogram.

A two electrode set-up was created by connecting both the counter lead and the reference lead of the potentiostat to a single (0.5 cm<sup>2</sup>) platinum plate. As an orientation, the sweep with a three electrode set-up and an Ag/AgCl reference electrode is plotted together with the two points measurements in Figure 3.4.

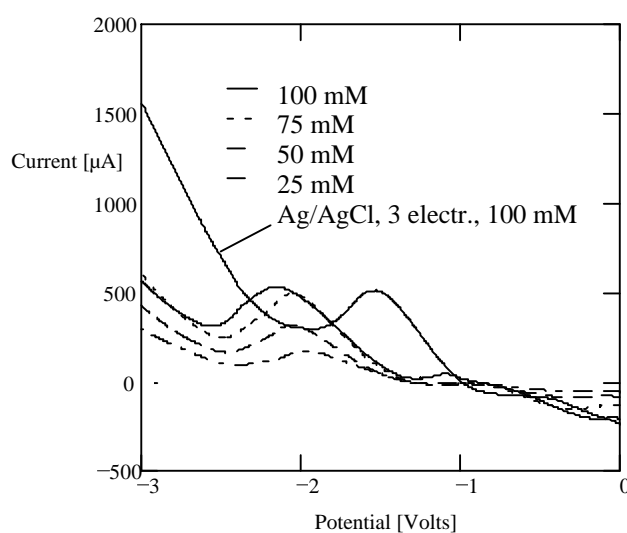


Figure 3.4: Potential sweep voltammograms in a two electrode system

The summary of all peak current versus concentration relations is plotted in Figure 3.5.

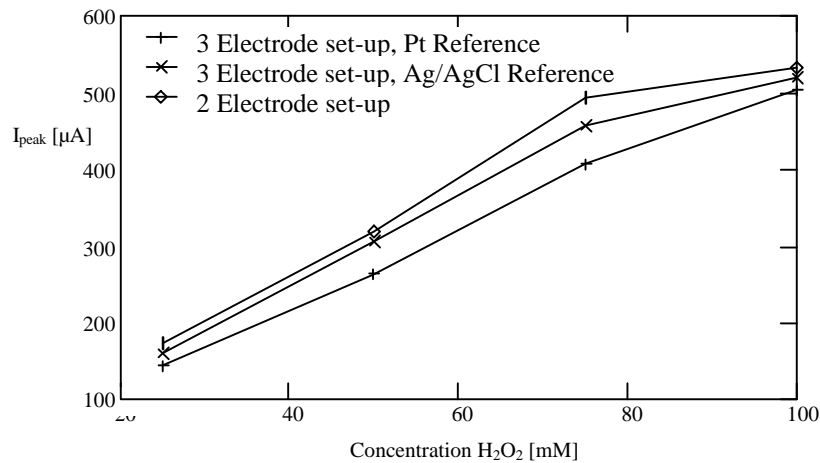


Figure 3.5: Summary of all measured  $I_{\text{peak}}$  - concentration relations

### 3.3 Conclusions

Potential sweep voltammetry appears to be a technique which does not need a decent reference electrode when only the concentration of a redox active component has to be measured. Decent reference electrodes are electrochemical half cells which show a concentration independent metal/electrolyte potential. In the described technique, this potential does not have to be well defined, but must at least remain constant during the potential sweep.

This technique can be used with either a three or two electrode system. The second one is more interesting because this can reduce the measurement probe to a simple stick with a small electrode on the upper side (for example the multi purpose integrated sensor structure) and a much larger platinum counter electrode on the back side.

## 4. Some additional comments on the conductivity-temperature technique

*In work report 10, concerning the ion concentration detection method using the conductivity versus temperature technique, some words were spent on the propagation of errors. However, there was no quantitative information provided on the size of these errors. Now, some additional measurements are performed to get an idea of the size and type of the errors in a conductivity measurement.*

### 4.1 Measurement of the error distribution curve

The simplification of the least square fitting algorithm as used in work report 10 is based on some assumptions. Because the discussion is in terms of mean, variance and covariance values, these statistic numbers must be measured to verify the assumptions.

#### *Theory*

The model which is used for the calculation of conductivities at several temperatures in a certain electrolyte is:

$$\bar{\Lambda} = \bar{\mathbf{B}} \cdot \bar{\mathbf{c}} + \bar{\mathbf{v}} \quad (4.9)$$

with

- $\bar{\Lambda}$  the vector containing the observations (measured conductivities at several temperatures),
- $\bar{\mathbf{B}}$  a matrix representing the system for calculating conductivities from ion concentrations using the applied temperatures,
- $\bar{\mathbf{c}}$  the input vector to be estimated consisting of all the separate ion concentrations and
- $\bar{\mathbf{v}}$  the noise or error in the measurement.

The aim is to find an estimate  $\hat{\mathbf{c}}$  for the vector  $\bar{\mathbf{c}}$  satisfying the observed vector  $\bar{\Lambda}$ . When the average of the estimate is the true value:

$$\mathbb{E}(\hat{\mathbf{c}}) = \bar{\mathbf{c}} \quad (4.10)$$

then the estimate is called unbiased. In the ideal case, the estimate is equal to the true value. In practice, however, an error will be present represented by the error vector:

$$\bar{\mathbf{e}} = \hat{\mathbf{c}} - \bar{\mathbf{c}} = \hat{\mathbf{c}} - \mathbb{E}(\hat{\mathbf{c}}). \quad (4.11)$$

The estimation algorithm which was used in work report 10, uses a least square algorithm for minimising this error vector. The algorithm was valid when the following assumptions were made:

- $\bar{\mathbf{c}}$  and  $\bar{\mathbf{v}}$  are uncorrelated (the moment matrix  $\bar{\mathbf{C}}_{\bar{\mathbf{c}}\bar{\mathbf{v}}} \equiv \mathbb{E}(\bar{\mathbf{c}}\bar{\mathbf{v}}^T)$  is equal to zero);
- the elements of  $\bar{\mathbf{v}}$  are uncorrelated and have equal standard deviations  $S_v$ ;
- the true state of  $\bar{\mathbf{c}}$  is unknown so its moment matrix satisfies  $\bar{\mathbf{C}}_{\bar{\mathbf{c}}} \equiv \mathbb{E}(\bar{\mathbf{c}}\bar{\mathbf{c}}^T) \rightarrow \infty$ ;

These assumptions will be verified by some error measurements.

### Experimental

During some hours, a commercial conductivity meter (Radiometer CDM 210) was used for monitoring temperature and conductivity in stirred KCl solutions. The solution was heated and cooled down several times between room temperature (18 °C) and about 55 °C. In a spreadsheet program, the data was collected and compared to the theoretical conductivities for these temperatures.

Table 4.1: Statistical information of KCl conductivity measurements

Real concentration KCl [mM]	Measured conductivity (20 °C) [mS/cm]	Meter range [mS]	Mean error [mS/cm]	Standard deviation of error [mS/cm]
90	12.6	40	0.0009	0.05
309	38.5	400	0.0053	0.49
413	55.3	400	0.0183	0.50
615	86.2	400	0.0059	0.53

Notice that the conductivity meter switched to the 40 mS range for the first sample which corresponds to a fixed operational frequency of 23.4 kHz, and to the 400 mS range for the other three samples (46.9 kHz). Obviously, the standard deviation is dependent on the chosen operational frequency and not to the electrolyte concentration. However, because the operational frequency is chosen according to the electrolyte concentration, the standard deviation is indirectly dependent on this concentration in practical applications.

All the measured errors of the three samples measured with the 400 mS range were collected into a single error distribution plot (Figure 4.1) which approaches the normal distribution shape.

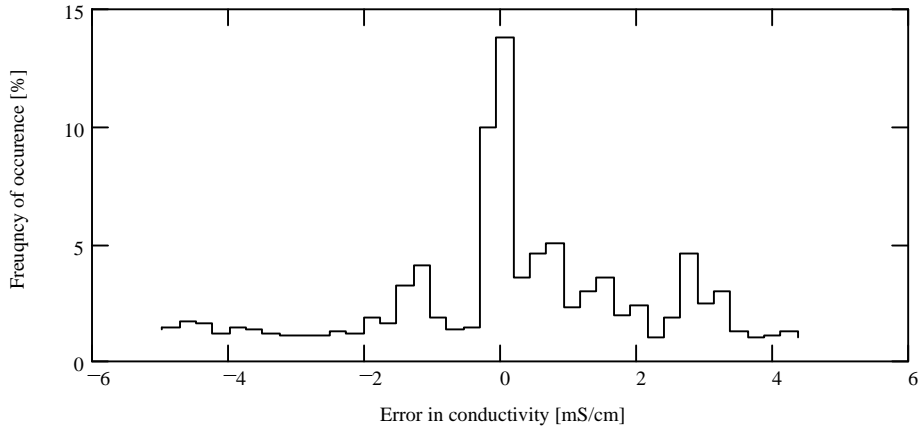


Figure 4.1: Error distribution in conductivity measurements

### Discussion

Comparing column 4 to column 2 in Table 4.1 it appears that the mean of the error is much lower than the observed conductivities. In other words:

$$E(\bar{v}) = 0$$

which implies directly that the covariance with  $\bar{c}$  is equal to zero as well:

$$\text{Cov}(\bar{c}, \bar{v}) = \overline{\bar{c}\bar{v}} \equiv E(\bar{c}\bar{v}^T) = 0$$

which proves the first assumption of  $\bar{c}$  and  $\bar{v}$  being uncorrelated.

The other two conditions are necessary to ensure that the moment matrix for  $\bar{c}$  is much larger than the moment matrix for  $\bar{v}$ :

$$\overline{\overline{C_c}} \rightarrow \infty \text{ and } \overline{\overline{C_v}} \rightarrow 0, \text{ or } \overline{\overline{C_c}} \gg \overline{\overline{C_v}}$$

Since the standard deviations of  $\bar{v}$  are finite and known (fifth column of Table 4.1), its moment matrix will be small. More correctly: its moment matrix will go to zero in relation to the corresponding moment matrix for  $\bar{c}$ , which will go to infinite because its covariance goes to infinite [4].

The value for the standard deviation appears to be constant (about 0.5 mS/cm) with the exception of the first electrolyte measurement which is a factor ten smaller. This means that about 95% of the conductivity measurements is between the real conductivity plus/minus two times this standard deviation for the chosen operational range.

Besides being dependent on the operational frequency of the conductivity meter, the standard deviation might be dependent on temperature. Therefore the data of the three measurements in the 400 mS range, was split into four sets: lower than 30 °C, lower than 40 °C, lower than 50 °C and higher than 50 °C. The calculated standard deviations are in Table 4.2.

Table 4.2: Standard deviations calculated in several temperature ranges

Temperature range [°C]	Standard deviation [mS/cm]
< 30 °C	0.31
30 °C . . 40 °C	0.36
40 °C . . 50 °C	0.40
> 50 °C	0.42

Although there is a small temperature dependency, no big error is introduced when assuming a temperature independent standard deviation.

## 4.2 Absolute errors in the fitted ion concentrations

Now the standard deviations of the errors are known, the absolute errors in the calculated concentrations can be calculated. The complete model is:

$$\begin{bmatrix} \Lambda_1 \\ \Lambda_2 \\ \vdots \\ \Lambda_N \end{bmatrix} = \begin{bmatrix} \sum_{j=0}^J k_{1,j}(T_1 - T_0)^j & \sum_{j=0}^J k_{2,j}(T_1 - T_0)^j & \cdots & \sum_{j=0}^J k_{i,j}(T_1 - T_0)^j \\ \sum_{j=0}^J k_{1,j}(T_2 - T_0)^j & \sum_{j=0}^J k_{2,j}(T_2 - T_0)^j & \cdots & \cdot \\ \vdots & \vdots & \ddots & \vdots \\ \sum_{j=0}^J k_{1,j}(T_N - T_0)^j & \cdot & \cdots & \sum_{j=0}^J k_{i,j}(T_N - T_0)^j \end{bmatrix} \begin{bmatrix} |z_1|c_1\lambda_1^0 \\ |z_2|c_2\lambda_2^0 \\ \vdots \\ |z_i|c_i\lambda_i^0 \end{bmatrix} \quad (4.12)$$

with

$L$  the measured conductivities [S/m];

- $k_{i,j}(T_n-T_0)$  temperature dependency terms for ion  $i$ , power  $j$  and temperature  $n$  [together dimensionless];  
 $z_i$  ion charge for ion  $i$  [no dimension];  
 $c_i$  the concentration of ion  $i$  [mole/litre];  
 $l_i^0$  limiting molar ionic conductivity [ $m^2 S \text{ mole}^{-1}$ ];

The propagation of errors from the measured conductivity to the calculated concentrations is given by the moment matrix:

$$\overline{\overline{C}}_c = \left( \overline{\overline{B}}^T \overline{\overline{B}} \right)^{-1} \cdot \sigma_v^2 \quad (4.13)$$

when the estimation algorithm as presented in work report 10 is used. In this equation the matrix  $\overline{\overline{B}}$  is the matrix with the temperatures and coefficients  $k_{i,j}$  from equation (4.12), and  $S_v$  the standard deviation of the conductivity measurement. The moment matrix contains the variances of the  $|z|c|$  <sup>0</sup>-vector on its diagonal, and the covariances of this vector on the non-diagonal entries. So, when the error of a certain value is given by two times its standard deviation (95% probability region), the resulting absolute error in the fitted ion concentration will be:

$$e_{c,i} = \frac{2\sigma_v}{|z_i| \lambda_i^0} \sqrt{\left( \overline{\overline{B}}^T \overline{\overline{B}} \right)^{-1} \Big|_{i,i}} \quad (4.14)$$

with

- $e_{c,i}$  the absolute error in the fitted ion concentration for ion  $i$  [mole/litre];  
 $z_i$  the ionic charge for ion  $i$  [no dimension];  
 $l_i^0$  limiting molar ionic conductivity [ $m^2 S \text{ mole}^{-1}$ ];  
 $\overline{\overline{B}}$  the matrix with the temperatures and coefficients  $k_{i,j}$ ;  
 $S_v$  the standard deviation in the measured conductivity [S/m];

With this equation, errorbars can be drawn in previously measured concentration plots. For example, Figure 4.2 is repeated from work report 10, Figure 4.5, but now with errorbars and plotted in two separate graphs.

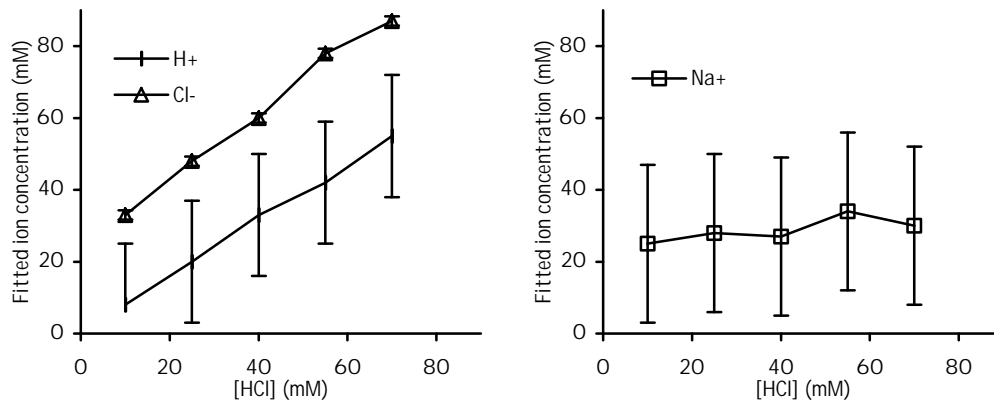


Figure 4.2: Fitted ion concentrations in solutions with 25 mM NaCl and several HCl concentrations from left to right: 10 mM, 25 mM, 40 mM 55 mM and 70 mM

Equation (4.14) shows that the error is not equal for each ion: for sodium 22 mS/cm, for hydrogen 17 mS/cm and for chloride 1.3 mS/cm. The error for hydrogen is smaller than the error for sodium because hydrogen has a more distinctive shape of its

temperature curve. Because the zero charge criterium was used, the error for chloride is much smaller than the other two.

This mathematical tool for calculating the error in the fit gives the possibility of qualifying the effect of the introduction of the zero charge criterium and the effect of the increase of the number of measured temperatures. However this calculation was not yet done.

## 5. Future work

*Now the integrated sensor array is being reduced to a single dip stick with a pseudo reference/counter electrode on the back side, an interesting device for writing a complete thesis on this subject is available. In this section I would like to give an overview of what chapters and topics will be in this thesis and what research still has to be done before this thesis can be completed.*

### 5.1 What has to be done

#### *Testing the final batch of sensors*

At this moment, a final batch of integrated sensors has been processed. A new batch was necessary because some calculations concerning the thermoresistive heating showed that the silicon substrate absorbed the heat before the electrolyte was heated. The new sensors are placed on a Hoya (glass) substrate which has thermal properties which resemble water. The measurements carried out with the silicon based structures should be repeated to show this improvement.

#### *Finishing the measurements for the conductivity versus temperature technique*

The theory for the ion fitting algorithm is well described, including the concepts of error propagation. In addition, this technique was verified for simple electrolytes using commercially available tools (conductivity meter and heater). However, up till now, the integrated sensor array itself was not yet used for doing such a experiment. For a coherent thesis this must be done.

A single test using a (glass) sensor structure was done. After the local environment was heated, the cooling down was recorded together with the electrolyte conductivity, all done using the same integrated sensor structure. Because the performance and interpretation of these measurements would take too much time, a student will be brought in by Unilever for doing this.

#### *Testing PCB structures*

Besides the successful silicon technology sensor structures, some cheaper versions which consist of gold plated copper layers on standard printed circuit boards were created. Some simple tests were already done, but a complete characterisation was not yet performed.

#### *On line precipitation titration of calcium ions*

The most interesting application of the integrated device is the sensor/actuator operation referred to as conductivity versus temperature technique. In addition, a second sensor/actuator method can be performed. When a local bump of hydroxide ions is created by the electrolysis of water, the response of the electrolyte on this local pH change can be monitored using the device as a conductivity sensor.

So it might be possible to detect the end point of a titration of calcium with hydroxide ions by monitoring the electrical conductivity. Figure 5.1 shows a very preliminary test measurement of a volumetric (using a burette) titration monitored by a

commercial conductivity meter. The end point of the titration appears as a local maximum in the electrolyte resistivity, from the applied amount of titrant at this end point the calcium concentration can be calculated.

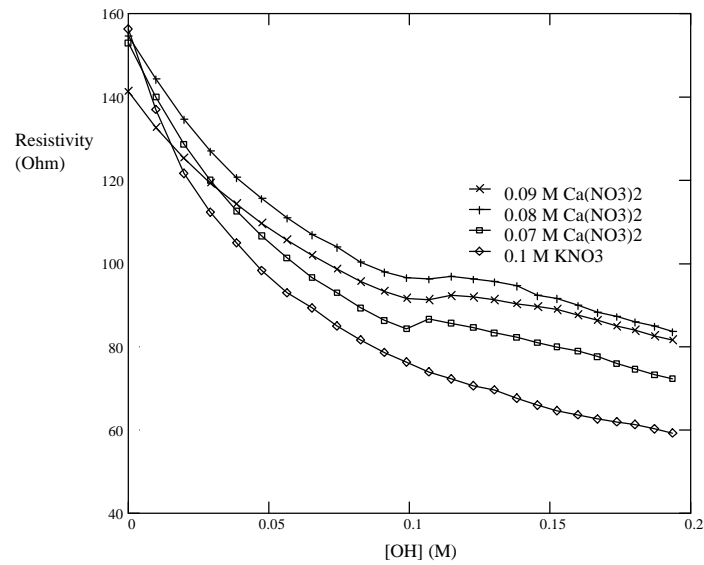


Figure 5.1: Very preliminary measurements for a volumetric precipitation titration of calcium with sodium hydroxide

When this technique can be repeated using the integrated sensor/actuator array, a second very interesting analytical method is available.

#### *Turbulence (flow) detection*

A third actuator/sensor operation is achieved by heating the local environment while monitoring the local temperature. Since the movement of the liquid medium limits the temperature elevation, an indication of the turbulence is given. A simple experiment can be done by recording the temperature using one resistive branch of the structure while heating with the other. With a stirrer the turbulence of the medium can be controlled.

## 5.2 Outline of the thesis

From the work that was done up till now, and the few things that still have to be done, the following intended outline of the thesis was constructed:

Title: **Integrated sensor arrays for monitoring washing processes**

### **Chapter 1: Overview**

#### *Washing systems*

This section describes why sensors should be integrated with washing machines and processes. Overview of existing machines with sensors.

#### *Sensor arrays*

Why should sensors be integrated and miniaturised. Separation into partial problems: the environment to be measured, the sensor structure, the control circuitry, interpretation of data and sensor- actuator responses

### **Chapter 2: Specifications of the washing environment**

#### *Measurable versus process parameters.*

*Selection of washing parameters* which should be implemented in the sensor array.

*Ranges* of values that can be expected.

*Example* of the relation between observed water hardness and measured conductivity in tap water (from statistical data of Dutch drinking water).

### **Chapter 3: Sensor materials and principles**

Based on work report 5. Sensor classification of existing sensor techniques based on sensor materials, measured parameter and type of measuring device. The conclusion will be that most of the parameters of interest can be measured using simple metal films.

### **Chapter 4: The integrated multi-purpose sensor array**

Design and characterisation of integrated sensor array for three sensor operations and two actuator operations (as described in reports 8 and 9 and published at the Transducers '97 conference). Design and measurements

### **Chapter 5: Amperometry for bleach detection**

(based on chapter 2 and 3 of this report)

pourbaix diagram, elimination of reference electrode

### **Chapter 6: Heating**

Temperature measurement and control (thermal diffusion model, analogy with electrical transmission line and ion diffusion);

Turbulence detection.

Including measurements as described in report 8 and 9.

### **Chapter 7: Sensor/actuator systems**

Based on work report 7. When making a table with the available actuator operations versus the available sensor operations, a lot of possible new parameters will be found. This systematic method will show the coherence of the following chapters with existing sensor actuator systems (coulometric micro titrator, time of flight flow sensor, etc.)

### **Chapter 8: Ion concentration determination by heating while monitoring the conductivity**

Theory, measurements, estimation algorithm.

### **Chapter 9: Precipitation titration of calcium**

Theory, model, measurements.

**Chapter 10: Supplementary results**

PCB sensor structures and last minute results

**Chapter 11: Conclusions and recommendations**

So, besides reporting the development and characterisation of the sensor-actuator device, the thesis can be a nice reference book and starting point for other researchers in the field of some basic electrolyte characterisation techniques.

## A. References

- [1] M. Pourbaix,  
Atlas of electrochemical equilibria in aqueous solutions,  
Pergamon Press, 1966.
- [2] D.R. Leide, H.P.R. Frederikse,  
Handbook of chemistry and physics, 74<sup>th</sup> edition 1993-1994,  
CRC Press, Inc., Boca Raton, Florida, 1993.
- [3] A.J. Bard and L.R. Faulkner,  
Electrochemical methods, fundamentals and applications,  
John Wiley and Sons, Inc., New York 1980.
- [4] P.B. Liebelt,  
An introduction to optimal estimation,  
Addison-Wesley Publishing Company, Reading, Massachusetts, 1967

## B. Distribution list

P. Bergveld (UT EL BIO)  
W. Olthuis (UT EL BIO)  
A.P.A.F. Rocourt (URL)  
M.M.C.G. Warmoeskerken (URL, UT CT)  
J.P. Janssens (URL)  
Remko Boom (URL)  
Henk Leeuwis (3T BV)